A MRI PHANTOM FOR CARDIAC PERFUSION SIMULATION

*Santiago Aja-Fernández, Lucilio Cordero-Grande, Carlos Alberola-López**

LPI, ETSI Telecomunicación, Universidad de Valladolid, Spain

ABSTRACT

This paper describes a realistic cardiac MR perfusion simulator; both the kinematic model of the perfusion process as well as breathing effects are described and a novel model for the AIF is proposed. Additionally the most common degradation factors involved in the MR image formation, such as those derived from parallel acquisition protocols, the presence of thermal noise and its correlation, the partial volume effect, the field inhomogeneity and the image saturation, are also incorporated into the simulation. Resulting images show a strong resemblance with natural images and perfusion curves obtained seem parallel to those that could be observed in a real setting.

***Index Terms*—** magnetic resonance, phantoms, noise, cardiac perfusion.

1. INTRODUCTION

Comparison of different algorithms in medical image processing is an issue since results are reported for different cohorts of patients, inclusion criteria, imaging equipment and so forth. In addition, determination of the ground truth may also constitute a matter of discussion, since inter and intra observer variability cannot be neglected. Therefore, simulators constitute a valuable tool to that end, as well as a simple tool to find out about the algorithm behavior under controlled circumstances. As a consequence, different simulators have been reported in different application domains, such as MRI [1] and diffusion tensor imaging [2] for the brain, or heart motion [3, 4], just to mention a few.

Dynamic-contrast enhanced MRI images [5] are often used to determine myocardium characterization after an ischemic episode has taken place. In this paper we are interested in perfusion images of the heart obtained after an injection of gadolinium. Different physical models have been developed for perfusion, so efforts for standardization have also been described [6]. In addition, different proposals exist for estimating the parameters of the kinetics involved [7], which are then used to classify tissues into different pathological stages.

In this paper we describe a realistic simulator that can help compare processing algorithms and, specifically, different estimation procedures of the parameters of the kinetic model in cardiac MRI perfusion images. To that end, we use a well-known compartment model, although the arterial input function (AIF) we here propose is slightly more involved than the simple model used elsewhere [7]. In addition, realistic MRI acquisition procedures have been simulated.

2. A CARDIAC MR PHANTOM

2.1. Perfusion model

In order to simulate the perfusion of Gadolinium to the tissues, a perfusion model must be adopted. We have assumed the following differential equation [6]:

$$\frac{dc(t)}{dt} = K_T\, c_a(t) - K_e c(t) \tag{1}$$

where $c_a(t)$ is the concentration of Gadolinium in the blood (the so-called AIF), $c(t)$ is the concentration of Gadolinium in the tissue, and K_T and K_e are constants (expressed in min$^-$1), the values of which depend on the tissue itself.

From eq. (1), assuming initial rest, the solution $c(t)$ turns out to be the convolution of $c_a(t)$ with an impulse funtion $r(t) = K_T e^{-K_e t} u(t)$, with $u(t)$ the Heaviside step function. The AIF has been modeled as a Gamma distribution

$$c_a(t) = M_1 \cdot \frac{t^{a-1} e^{-t/b}}{\Gamma(a) b^2} u(t) \tag{2}$$

with M_1 a normalization constant and a and b the shape and amplitude parameters, respectively, of the Gamma function; yet simple, this approximation shows more flexibility than the bi-exponential model sometimes used [7], which only approximates the decaying part of the perfusion process. More involved models may be used, such as a linear combination of Normal or of Gamma distributions; in fact, in Fig. 1-(a) an example of the AIF model with one Gamma is shown. Although the shape may fit a real AIF, the final state differs. In Fig. 1-(b) a more realistic model is obtained by using two Gamma distributions.

*This work was partially supported by the Ministerio de Ciencia y Educación and FEDER under Research Grant TEC2010-17982, and by the CDTI under the cvREMOD project and Research Grant CEN-20091044. The work was also funded by the Junta de Castilla y León under Grants VA376A11-2 and the Consejería de Sanidad de Castilla y León under Grants SAN126/VA032/09 and SAN126/VA033/09.

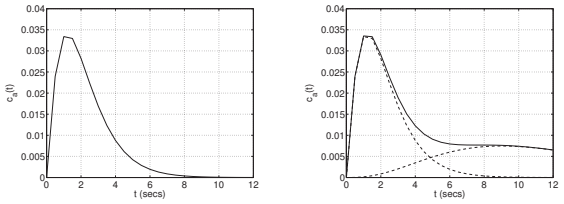


Fig. 1. Gamma model for continuous AIF simulation. Left: One Gamma model. Right: Two Gamma model.

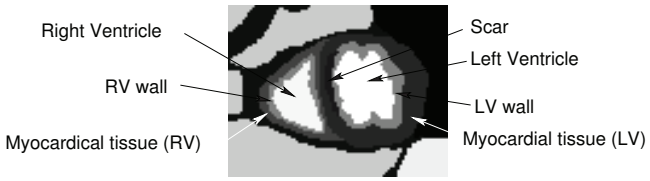


Fig. 2. Different tissues considered in the phantom. The image is created from a segmented real MR acquisition.

The concentration in the tissue, $c(t)$ is obtained via the analytical convolution with $r(t)$:

$$c(t) = M_1 \cdot r(t) \cdot \frac{\gamma_i\left(a, t\left(\frac{1}{b} - K_e\right)\right)}{(1 - K_e \cdot b)^a} \tag{3}$$

with $\gamma_i()$ the incomplete Gamma function. The concentration of blood and tissue in each point will be given by the discrete sampling of the continuous values in eq. (2) and eq (3), i.e. $c_a(n\Delta t)$, $c(n\Delta t)$.

2.2. Definition of areas of interest

As a seed point, a segmented cardiac image from a real acquisition is considered, as shown in Fig. 2. The main areas considered are the left and right ventricles, where the wall and the tissues are differentiated. A scar is also defined in the myocardial tissue. This initial image can be changed if needed.

To further simulate the perfusion, each tissue is assigned a different initial gray level, taken the average values found in these kind of sequences: assuming a dynamic range between [0-255], the myocardial tissue is initially set to 32, blood to 240 and air to 0.

2.3. Simulation of the MR acquisition

Let $I_0(\mathbf{x})$ be the original synthetic image as defined in the previous section. This image is to be corrupted in order to replicate the procedure in a MR acquisition. To that end, the following options were considered:

Perfusion sequence scans: Each area within the original image is assigned a pair of perfusion parameters (K_T and K_e). Only the right and the left ventricles, the blood and the scar will be affected by perfusion. The area of blood inside each ventricle is modeled using the AIF defined in eq. (2) with some delay between ventricles. The perfusion in the endocardium and scar are modeled using eq. (3).

The total number of scans N_t and the sampling time Δt must be defined. The concentration of Gadolinium in each point of the image is calculated using eq (3) and the particular values of the parameters, so a concentration value for each point and each time instant is obtained, i.e., $c_n(\mathbf{x}) = c(n\Delta t),\ \ n = 0, \cdots, N$.

From the concentration we create the T1 maps using

$$\frac{1}{T_1} = \frac{1}{T_{10}} + c_n \cdot r_1 \tag{4}$$

with T_{10} the T_1 value before the contrast injection and r_1 a relaxitivity parameter expressed in l/s/mmol; then the signal images are obtained assuming the following model

$$I_n(\mathbf{x}) = M_0\left(1 - e^{-\frac{T_R}{T1_n(\mathbf{x})}}\right),\ \ n = 0, \cdots, N. \tag{5}$$

Acquisition coils: The phantom can be acquired in a single coil scanner or using a multiple coil head. In the case of single coil, the synthetic image $I_n(\mathbf{x})$ is corrupted with complex Gaussian noise with zero mean and variance σ_n^2. The envelope is calculated, resulting that the signal $M_n(\mathbf{x})$ is Rician-distributed [8].

If multiple coils are considered, the image at the l-th coil $I_n^l(\mathbf{x})$ is obtained by multiplying $I_n(\mathbf{x})$ by a simulated sensitivity map $S_l(\mathbf{x})$ of the coil. The maps are designed so that the Sum of Squares (SoS) [10] in index l is one. An example of these simulated sensitivity maps is given in Fig. 3. In addition, data in each coil is corrupted with complex additive Gaussian noise with covariance matrix $\mathbf{\Sigma}$ [9]. If this matrix is not diagonal, correlation is assumed between coils, which is closer to reality. If no acceleration is assumed, the composite magnitude signal is obtained using SoS:

$$M_n(\mathbf{x}) = \sqrt{\sum_{l=1}^{L} |I_n^l(\mathbf{x}) + n_r^l(\mathbf{\Sigma}) + j n_c^l(\mathbf{\Sigma})|^2}$$

resulting in a non-central Chi [10] model. Examples of acquisitions are shown in Fig. 4 and Fig. 5.

Parallel imaging: When multiple coils are considered the acquisition may be accelerated by subsampling the **k**-space. In the phantom, subsampling and reconstruction with SENSE [11] and GRAPPA [12, 13] is available for simulation. Examples of parallel acquisitions are shown in Fig. 5.

Spatially correlated noise: The noise added in the single and multiple coil simulation can also be spatially correlated. Examples are shown in Fig. 4.

Partial Volume Effect (PVE): Due to the resolution in MR scans, there are voxels in which different tissues are mixed up. To simulate this effect, a convolution of the original image with a Gaussian kernel G_{σ_g} is used:



Fig. 3. Synthetic sensitivity map for an 8-coil system, created so that the SoS of the maps gives a constant image.



(a) (b) (c) (d) (e)

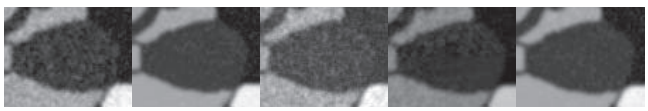
Fig. 4. Example of noise corruption assuming a single coil acquisition. (a) Original synthetic image. (b) Image corrupted with Rician noise, $\sigma_n = 20$. (c) Image corrupted with Rician noise, $\sigma_n = 20$ assuming that the noise is spatially correlated. (d) Rician noise ($\sigma_n = 10$) assuming spatial correlation and Partial Volume Effect ($\sigma_g = 1.5$). (e) Rician noise ($\sigma_n = 10$), spatial correlation, PVE and an inhomogeneous field.

Breathing movement: One of the main problems when analyzing heart MR data is the mismatch of the different images due to the breathing movement (as well as the heart movement itself). This motion is simulated by using a random affine transformation. An example is shown Fig. 6.
Field inhomogeneity: Image $I_n(\mathbf{x})$ is multiplied by a non uniform illumination $F\mathbf{x}$. An example is shown in Fig. 4-(e).
Saturation: Some acquisition schemes are designed to saturate the signal in the image. A maximum value can be set, so that the image is cropped to that value $\mathcal{S}_{\max}$:

$$M_n^{\mathcal{S}}(\mathbf{x}) = \min\{M_n(\mathbf{x}), \mathcal{S}_{\max}\}$$

3. SIMULATION AND EXPERIMENTS

For the sake of illustration some experiments and examples of the phantom behavior are now described.



(a) (b) (c) (d) (e)

Fig. 5. Multiple coil acquisition simulation. All the examples are spatially correlated, assuming PVE and $\sigma_n = 10$ in each coil. (a) Single coil acquisition. (b) 8-coil acquisition, no correlation between coils. (c) 8-coil acquisition assuming a coefficient of correlation between coils $\rho^2 = 0.1$. (d) 8-coil acquisition with $\rho^2 = 0.1$, a 2x subsampling of the **k**-space and SENSE reconstruction. (d) 8-coil acquisition with $\rho^2 = 0.1$, a 2x subsampling of the **k**-space and GRAPPA reconstruction.

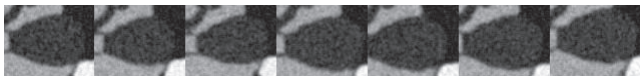
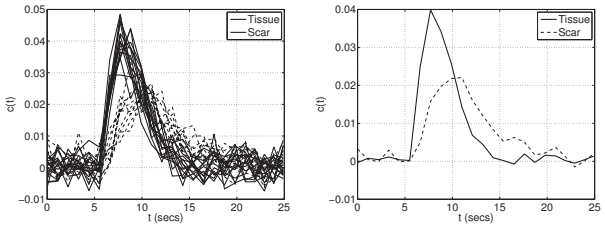


Fig. 6. Simulation of the breathing movement in a single slice.



(a) Individual points (b) Averaged

Fig. 7. Simulation of the perfusion: estimated concentration of Gadolinium in tissue. Estimated from simulated MR single coil acquisition with $\sigma_n = 10$. (a) Selection of points (b) Average for all the points in each tissue (obtained by clustering).

First, to illustrate the importance of *degradation* in MR if realistic images are to be generated, we create a simple perfusion sequence. Noise is not added and no PVE or breathing movement are accounted for. We consider $N = 17$ images with a sampling rate of $\Delta t = 2.5$ secs, $r1 = 4.5$ TR$= 2.7290$ (msec) and we define the myocardial tissue with $K_T = 0.8$ and $K_e = 0.3$; the scar is modeled with $K_T = 0.5$ and $K_e = 0.4$. Results are shown in Fig. 8-top. The the effect of the perfusion within the tissue and blood is simulated. However, the resulting image is far from a real MR acquisition.

More realistic images can be obtained via a controlled degradation of the data. Using the same perfusion parameters, the image is now assumed to be Rician, from a single-coil acquisition. Noise with $\sigma_n = 15$ is added to the complex **x**-space, the breathing movement is simulated, and finally, PVE and an inhomogeneous field are considered. The resulting sequence (Fig. 8, two bottom lines) is now much closer to what a real perfusion MR sequence looks like.

The concentration $c(t)$ curves are estimated from the data in the myocardial tissue and in the scar. For a clearer illustration new images are generated with $\sigma_n = 10$, $N = 20$, $K_T = 0.1.3$ (tissue), $K_T = 0.5$ (scar), $K_e = 0.8$ (tissue), $K_e = 0.4$ (scar). The $c(t)$ curves of a selection of points within the tissue and scar are shown in Fig. 7-(a). As an effect of the degradation the curves show a noisy behavior. To separate and average the curves belonging to each tissue a clustering algorithm (k-means) is used to search for the two final sets. The results are shown in Fig. 7-(b).

4. CONCLUSIONS

A realistic perfusion MR cardiac simulator has been described; different realistic effects on the perfusion process,

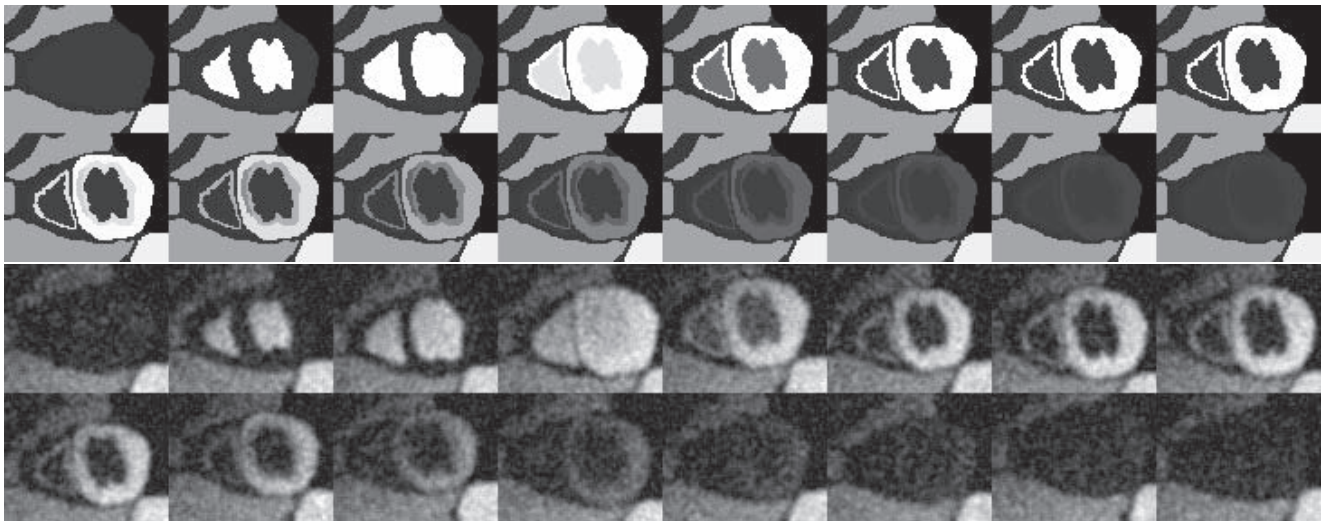


Fig. 8. Simulation of the perfusion with MR acquisition. $N = 16$, $\Delta t = 2.5$ sec., $K_T = 0.8$ (tissue), $K_T = 0.5$ (scar), $K_e = 0.3$ (tissue), $K_e = 0.4$ (scar). Top: No degradation of the image. Bottom: MR simulation, single coil adquisition, Rician noise ($\sigma_n = 15$), PVE, spatial correlation, inhomogeneous field and respiration movement.

breathing motion as well as on the MRI adquistion have been included. A novel AIF model has been proposed, which lets the designer model the perfusion procedure since the gadolinium onset until it is eventually washed out. Further research may focus on more realistic models for the AIF function here proposed.

5. REFERENCES

[1] D.L. Collins, *et al.*, "Design and construction of a realistic digital brain phantom," *IEEE Trans. Med. Imaging*, vol. 17, no. 3, pp. 463–468, June 1998.

[2] A. Tristán-Vega and S. Aja-Fernández, "Design and construction of a realistic DWI phantom for filtering performance assessment," in *MICCAI 2009, Lecture Notes in Computer Science*, 2009, vol. 5761, pp. 951–958.

[3] A.I. Veress *et al.*, "Normal and pathological NCAT image and phantom data based on physiologically realistic left ventricle finite-element models," *IEEE Trans. Med. Imaging*, vol. 25, no. 12, pp. 1604–1616, Dec. 2006.

[4] W.P. Segars, D.S. Lalush, and B.M.W. Tsui, "A realistic spline-based dynamic heart phantom," *IEEE Trans. on Nuclear Science*, vol. 46, no. 3, pp. 503–506, June 1999.

[5] A. Hennemuth *et al.*, "A comprehensive approach to the analysis of contrast enhanced cardiac MR images," *IEEE Trans. Med. Imaging*, vol. 27, no. 11, pp. 1592–1610, Nov. 2008.

[6] P.S. Tofts *et al.*, "Estimating kinetic parameters from dynamic contrast-enhanced T1-weighted MRI of a diffussable tracer: Standardized quantities and symbols," *J. Magn. Reson. Imaging*, vol. 10, pp. 223–232, 1999.

[7] V. Schmid *et al.*, "Bayesian method for pharmacokinetic models in dynamic contrast-enhanced magnetic resonance imaging," *IEEE Trans. Med. Imaging*, vol. 25, no. 12, pp. 1627–1636, Dec. 2006.

[8] H. Gudbjartsson and S. Patz, "The Rician distribution of noisy MRI data," *Magn. Reson. Med.*, vol. 34, no. 6, pp. 910–914, 1995.

[9] S. Aja-Fernández and A. Tristán-Vega, "Influence of noise correlation in multiple-coil statistical models with sum of squares reconstruction," *Magn. Reson. Med.*, vol. 67, no. 2, pp. 580–585, Feb. 2012.

[10] C.D. Constantinides, E. Atalar, and E.R. McVeigh, "Signal-to-noise measurements in magnitude images from NMR based arrays," *Magn. Reson. Med.*, vol. 38, pp. 852–857, 1997.

[11] K.P. Pruessmann *et al.*, "SENSE: Sensitivity encoding for fast MRI," *Magn. Reson. Med.*, vol. 42, no. 5, pp. 952–62, Nov. 1999.

[12] M.A. Griswold, *et al.*, "Generalized autocalibrating partially parallel acquisitions (GRAPPA)," *Magn. Reson. Med.*, vol. 47, no. 6, pp. 1202–1210, 2002.

[13] S. Aja-Fernández, A. Tristán-Vega, and W.S. Hoge, "Statistical noise analysis in GRAPPA using a parametrized non-central chi approximation model," *Magn. Reson. Med.*, vol. 65, pp. 1195–1206, 2011.